EPR investigation of the intermediate spin exchange regime

Barney L. Bales and Dennis Willett

Citation: The Journal of Chemical Physics **80**, 2997 (1984); doi: 10.1063/1.447134
View online: http://dx.doi.org/10.1063/1.447134
View Table of Contents: http://scitation.aip.org/content/aip/journal/jcp/80/7?ver=pdfcov
Published by the AIP Publishing

EPR investigation of the intermediate spin exchange regime

Barney L. Bales and Dennis Willett[a)]

Department of Physics and Astronomy, California State University, Northridge, California 91330
(Received 3 May 1983; accepted 6 October 1983)

The electron paramagnetic resonance spectra of di-*tert* butylnitroxide (DTBN) are studied as a function of the nitroxide concentration in three hydrocarbon solvents at constant temperature. In the concentration range studied, DTBN undergoes electron spin exchange which leads to broadening, shifting, and eventual collapse of the lines forming the 19-line proton hyperfine pattern. Particular emphasis is given to the spin exchange frequencies ω_{HE} in the region in which they are comparable with the proton hyperfine coupling constants—the intermediate spin exchange regime. Both linewidths and line shapes are found to be in full accord with theory in the intermediate exchange regime which completes the demonstration that theory and experiment are in agreement, the slow and fast exchange regimes having been studied many times in the past. Modeling the spectral lines as Lorentzian–Gaussian convolutions allows a detailed exposition of the collapse of the hyperfine structure as ω_{HE} increases and this collapse, too, is well described by theory. Bimolecular spin exchange rate constants are compared with the prediction of simple hydrodynamic theory.

INTRODUCTION

The sometimes spectacular effects on spectra due to interconversion of spectrally distinct molecules has a rich background theoretically and experimentally.[1] The frequency of interconversion, when compared with the spectral line separation, may be divided into three domains depending upon whether the former is small, comparable, or large compared with the latter. These exchange frequency domains are called slow, intermediate, or fast, respectively. One familiar example of the exchange phenomenon in EPR is electron spin exchange between like radicals in liquids, the line separation being provided by hyperfine coupling. In this case, slow exchange is defined by $\omega_{HE} \ll a_j$, where ω_{HE} is the spin exchange frequency and a_j is the hyperfine coupling constant due to the jth nucleus. Intermediate and fast exchange are described by $\omega_{HE} \sim a_j$ and $\omega_{HE} \gg a_j$, respectively.

Theoretically, there are a number of treatments[2-9] of the spin exchange problem all of which predict that as the exchange frequency increases, the resolved spectral lines first broaden, then coalesce, and finally narrow. Experimentally, the slow exchange limit has been carefully studied[10-14] and the fast exchange limit has been investigated somewhat.[15] In both limits, theory and experiment seem to be in agreement. The purpose of the present paper is to carefully study the intermediate exchange region and to compare the results with theory.

PROFILE OF THE NITROXIDE SPIN EXCHANGE PROBLEM

To facilitate the discussion, we refer to Fig. 1 which shows the EPR spectrum of a hypothetical spin $\frac{1}{2}$ radical that is coupled to five completely equivalent[16] protons. A six-line spectrum is observed in the absence of spin exchange [Fig. 1(a)]. Introducing spin exchange such that $\omega_{HE} \ll a$ (slow exchange) produces Fig. 1(b) where the positions of the lines are largely unaffected but the lines are broadened. Careful inspection of Fig. 1(b) illustrates a well-known effect—lines of higher degeneracy are broadened less.[5,7,8] This is due to the fact that spin exchanges between radicals with identical quantum numbers produce no spectral effect, a situation that arises more frequently with radicals that are members of a subclass producing more degenerate lines. In the succeeding spectra of Fig. 1, ω_{HE} increases progressively from top to bottom. Figure 1 illustrates the qualitative trend mentioned above—the lines broaden [Figs. 1(b) and 1(c)], begin to approach one another [Fig. 1(c)],

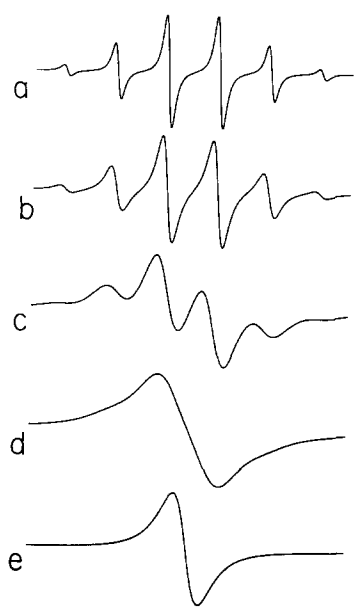

FIG. 1. Hypothetical EPR spectra due to hyperfine coupling to five equivalent spin one-half nuclei. The ratio of the spin exchange frequency to the hyperfine coupling constant varies from top to bottom $\omega_{HE}/a_e(0) = 0$, 0.11, 0.500, 1.00, and 3.33, respectively. The amplification factor varies from top to bottom 1.00, 2.71, 12.3, 15.4, and 4.92, respectively. The Lorentzian linewidth due to relaxation processes other than spin exchange is $2T_2^{-1}/3^{1/2}$ where $T_2^{-1}/a_e(0) = 0.111$ in each case.

a) Present address: Arco Solar Industries, P. O. Box 4400, Woodland Hills, CA 91365.

 0021-9606/84/072997-08$02.10

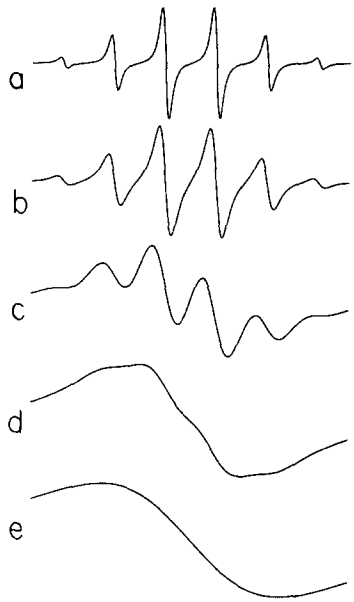

FIG. 2. One manifold of three-manifold hypothetical nitroxide EPR spectra showing hyperfine coupling to five equivalent spin one-half nuclei. The hyperfine coupling to the nitrogen nucleus would produce two other manifolds at a spacing two orders of magnitude larger than the spacings shown. The spin exchange frequency varies from top to bottom exactly as in Fig. 1.

coalesce [Fig. 1(d)], and finally, narrow [Fig. 1(e)]. In terms of Fig. 1, we may restate the situation: experimentally and theoretically the situations depicted in Figs. 1(b) and 1(e) are well understood. Our goal is to further the understanding of the situation depicted in Fig. 1(d).

Actually, the radical studied here presents a somewhat different situation than the hypothetical one suggested by Fig. 1 since, in addition to the hyperfine structure indicated, there is also a much larger hyperfine splitting due to coupling of the unpaired electron to a nitrogen nucleus. We study a nitroxide free radical because of its intrinsic importance and because of many desirable features that have been amply discussed.[1-7] In a typical nitroxide EPR spectrum, one observes three groups of lines in the motional narrowing regime, the groups being separated by about 15 G while line separations within any one of the three groups is on the order of several tenths of a Gauss. We use the term "manifold" to refer to a group of lines, corresponding to one value of the nitrogen nuclear quantum number $M_I = 0, \pm 1$.

A hypothetical manifold is shown in Fig. 2 using the same proton hyperfine pattern as that supposed in Fig. 1. As in Fig. 1, the exchange frequency is increased successively from the top of Fig. 2 to the bottom. The first three spectra of Figs. 1 and 2 are similar although there are quantitative differences, but the last two are quite different. Physically, the behavior is understandable in the two different cases—when the exchange frequency is small compared with both proton and nitrogen hyperfine spacings, the lines simply broaden without regard to the size of the spacings, so Fig. 1(b) is similar to Fig. 2(b). As the exchange frequency approaches the smaller (proton) hyperfine spacings, the lines tend to approach one another and coalesce in both cases but in the case of the nitroxide, exchanges with the other two manifolds continue to broaden the lines.

In this work we will be dealing with the intermediate spin exchange regime relative to the structure within a manifold (the proton splittings) while carefully remaining within the slow exchange regime relative to the nitrogen coupling. This latter restriction allows us to consider one manifold at a time undisturbed by appreciable overlap with the other two.

THEORY

The collapse of EPR structure with increasing radical concentration in liquids has been understood to be due to electron spin exchange interactions since the work of Pake and Tuttle.[3] Various theoretical techniques have been used to describe the phenomenon varying in sophistication from a simple Bloch equation approach to density matrix methods.[1-9] When applied to spin exchange between two nitroxides, as far as we can tell, all of the methods give the same results for the unsaturated linewidths in both the fast and slow exchange limits.

In the intermediate exchange limit Stillman and Schwartz[9] have shown that under conditions appropriate to nitroxides, the theories of Anderson[2] and of Freed[7,8] are identical. Johnson's theory[6] in turn is equivalent to Freed's. One other theory, due to Currin,[5] will be considered here.

Currin,[5] using a correlation function approach, derived an analytic solution to the spin exchange problem that is valid over the entire range of exchange frequencies from good hyperfine resolution to extreme narrowing employing only one parameter ω_{HE}. Currin's expression, modified to account for intrinsic linewidths, neglecting a small "stretching frequency" proportional to the mean lifetime τ_1 of the colliding pair is given in Eq. (1).

$$G(H) = \frac{N\sum \rho_j/[i(H-H_j)+\gamma(\omega_{HE}+T_2^{-1})]}{1-\omega_{HE}\sum \rho_j/[i(H-H_j)+\gamma(\omega_{HE}+T_2^{-1})]}, \qquad (1)$$

where ρ_j is the population of the jth hyperfine line normalized so that $\sum \rho_j = 1$. H_j is the resonant field of the jth line, $2T_2^{-1}$ is the width of the absorption lines in the absence of exchange, and N is the radical density. Small corrections due to the fact that the field is swept instead of the frequency are negligible and like all the other theories mentioned above, the pair lifetime is assumed to be small compared with all other characteristic times in the problem. The reader is referred to the literature for an exhaustive discussion of the assumptions involved in Eq. (1) and other formulations.[5-10] The first derivative of the real part of Eq. (1), which is proportional to the absorption derivative, is worked out in Appendix A.

We have chosen to emphasize Currin's theory because, even though it has been widely recognized to exist and to give results in agreement with other theories in the slow and fast exchange limits, it does not seem to have been used much. This is curious, because the Currin

TABLE I. Magnetic parameters for DTBN. $T = 30°C$.[a]

Solvent	a_N	$a_e(0)$[b]	T_2^{-1}[b]	$a(^{13}C_\alpha)$[c]	$a(^{13}C_\beta)$[c]	(^{13}C)[b]
mesitylene	15.34 ± 0.05	0.111	0.265	4.31	4.29	4.12
cis-decalin	15.21 ± 0.03	0.109	0.305	4.39	4.33	4.12
trans-decalin	15.18 ± 0.03	0.115	0.313	4.32	4.30	4.12

[a]All values in gauss.
[b]Values used in spectral simulation.
[c]Calculated from the empirical equations of Ref. 28.

formulation is very handy and may be easily programmed on a microcomputer to produce simulated spectra. In fact, the spectra in Figs. 1 and 2 were produced by the equations in Appendix A using an Apple II computer coupled to a Soltec digital plotter in a matter of a few minutes. By contrast, other methods, which often boil down to inversion of matrices of the order of the number of hyperfine lines can be quite unwieldy.

In the two extremes of good resolution and extreme narrowing, Currin's theory is identical to all the others.[5] Is Currin's theory compatible with other theories in the *intermediate* spin exchange regime? To answer this we have numerically compared the results obtained previously[18] from the theory of Freed[7,8] as applied by Stillman,[9] Schwartz, and the results from Currin's theory, and have found the linewidths to be identical throughout the intermediate exchange regime. In summary, even though they appear to be quite different, the various theories capable of predicting EPR spectra in the intermediate exchange region are in agreement at least under the conditions appropriate to the present experimental investigation.[19]

In dilute solution, spin exchange proceeds by bimolecular collision of the radicals, so ω_{HE} is proportional to the density of the radicals N. Thus

$$\omega_{HE} = K_e' N = K_e C \ , \tag{2}$$

which defines the spin exchange rate constant K_e, where C is the concentration in mol/ℓ. Experimentally, ω_{HE} may be controlled by varying N holding all other parameters constant.

We mention that for solutions in the viscosity range considered here, the spectral effects of electron–electron dipolar interactions are negligible.[12]

EXPERIMENTAL

The free radical di-*tert*-butylnitroxide (DTBN) was chosen for study. DTBN contains 18 equivalent protons giving 19 hyperfine lines of binomial intensity with approximately equal spacing. In hydrocarbons, $a_e(0)$ ~ 0.110 and the intrinsic linewidth is large enough in most cases that the hyperfine multiplet is unresolved even in the absence of spin exchange (see however Refs. 10 and 20). Table I gives magnetic parameters for DTBN.

The parameter ω_{HE} was varied experimentally by reducing the DTBN density N using a photoconversion technique described previously.[21] Briefly, samples prepared as described below were irradiated for short periods of time with a low-pressure mercury vapor lamp in order to photoconvert DTBN to a nonparamagnetic product. Repeated cycles of irradiation followed by spectral measurement leads to numerous spectra recorded as a function of N using a single sample (see Ref. 21 for further details).

DTBN, prepared according to the method of Hoffman,[23] was added volumetrically to mesitylene (99 +%), *trans*-decalin (99%), and *cis*-decalin (99%) to form 6 mM solutions. The solvents, purchased from Aldrich, were used as received. Samples were placed in 4 mm thin-wall glass tubes (Wilmad #412) to a height of 1.5 cm, passed through five freeze–pump–thaw cycles and sealed. Duplicate samples were prepared in each solvent and were stored in the dark at room temperature when not being irradiated or studied by EPR.

Careful temperature control at 30.00 ± 0.05 °C was achieved by passing thermostated transmission fluid through a quartz cavity insert of our design. Normal, careful procedures were employed in order to ensure good line shape reproduction as discussed previously.[21]

RESULTS

All of the results reported here are derived from the central nitrogen manifold in the EPR spectra of DTBN. At low radical concentration, a main, structureless line is observed, flanked by satellites due to ^{13}C in natural abundance, and other, less intense, satellites (see Refs. 10 and 24 for examples of EPR spectra of DTBN). Our concern is with the linewidth and line shape of the central main line as we vary ω_{HE} through the intermediate exchange region and some corrections need to be made to account for the presence of the ^{13}C lines. These corrections are discussed in Appendix B.

Figure 3 shows the total linewidth of DTBN in mesitylene as a function of the doubly integrated intensity which is, in turn, proportional to N. Relative values of the intensity were measured by a method developed in Ref. 18 as discussed in Ref. 21. In addition to the total linewidth, Fig. 3 shows the results of a deconvolution of the line into its Lorentzian and Gaussian components as described below.

The dashed line in Fig. 3 was generated by the theory of Currin. We note that simulations for DTBN were also carried out in Ref. 25. The proton hyperfine coupling constant at $\omega_{HE} = 0$, $a_e(0)$, and T_2^{-1} were measured from spectra at very low concentrations as before[18] and K_e was fixed by applying Eq. (2) in the fast exchange limit. These parameters, fixed outside the intermediate

spin exchange regime (Table I) were then used in the equations of Appendix A to generate the line in Fig. 3. It is seen that the agreement is excellent even through the region of large nonlinearity. The data for DTBN in *trans*-decalin are given in Fig. 4. In *cis*-decalin the data are similar.

Actually, a sensitive test of the DTBN linewidth dependence on ω_{HE} has been carried out before in a different context.[21] A table of linewidth vs ω_{HE} (spanning the pertinent parameters) was generated using Freed's theory.[7-9] The table was accurately represented by an empirical equation which, when applied to the experimental linewidths, yielded experimental ω_{HE}. The values of ω_{HE} were found to be accurately linear with N as shown in Figs. 2–4 of Ref. 21 thus confirming, in another way, and with a different formulation of the theory, the correctness of the theoretical prediction of the linewidth vs ω_{HE}.

We now turn to the dependence of the line shape on ω_{HE} in the intermediate exchange range. Since the line is accurately represented as a convolution of a Lorentzian (due to spin relaxation) and a Gaussian (due to unresolved hyperfine structure) at ω_{HE} = zero,[18] and since the hyperfine structure collapses at high ω_{HE}, we compare the experimental line shapes with those predicted by theory by comparing the Gaussian (Lorentzian) character of those lines.

Recently, we have formulated[18] methods to deconvolute EPR lines that are Gaussian–Lorentzian mixtures. The reader is referred to the literature for details,[18] but briefly, we exploit the fact that the intensity of the spectrum in the wings of a Gaussian and a Lorentzian differ appreciably. A parameter ψ was introduced [see Fig. 3, Ref. 18(b)] which is a measure of the spectral intensity in the wings—for a Gaussian $\psi^G = 0.067$ and for a Lorentzian $\psi^L = 0.213$. From the second moment of the hyperfine pattern, the Gaussian linewidth ΔH_{pp}^G was de-

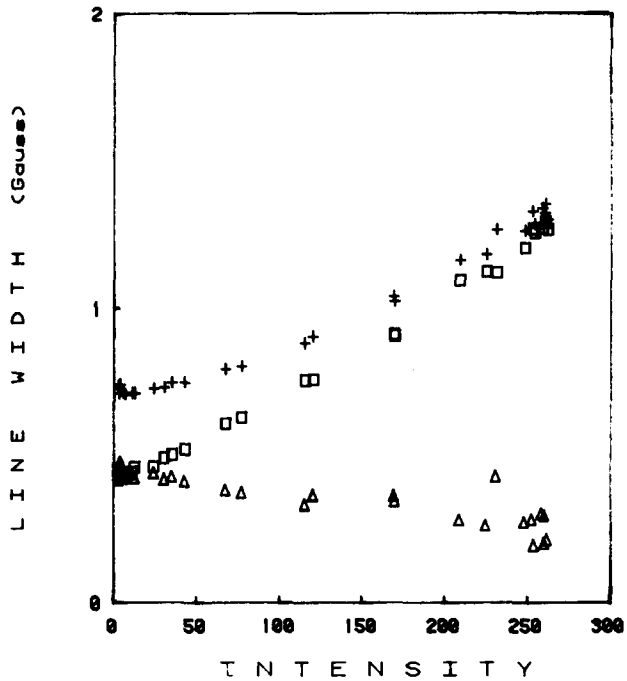

FIG. 4. Linewidth parameters for the $M_I = 0$ manifold of DTBN in *trans*-decalin. The symbols have the same meaning as in Fig. 3. $T = 30.00$°C.

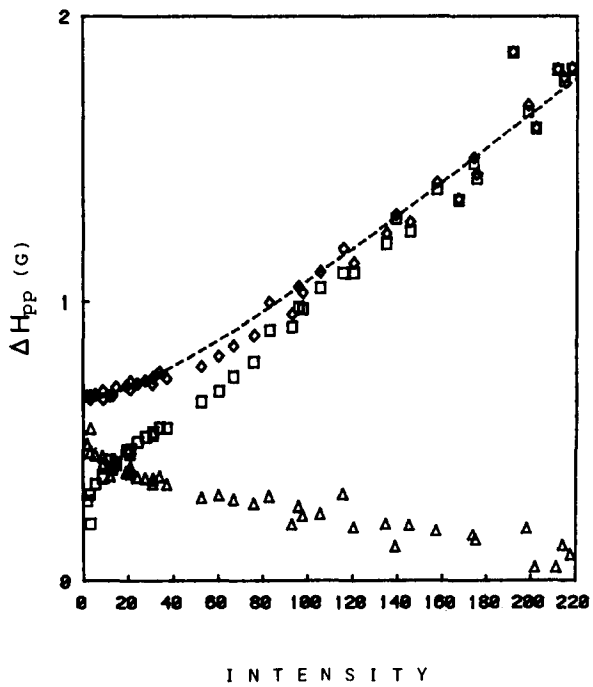

FIG. 3. The linewidth of the $M_I = 0$ manifold of DTBN as a function of the doubly integrated EPR spectral intensity. The line is the theoretical prediction for the total linewidth and the experimental points are given by ◊. Deconvolution gives the Lorentzian component linewidths ΔH_{pp}^L(□); and Gaussian component linewidths, ΔH_{pp}^G(Δ). Mesitylene, $T = 30.00$°C.

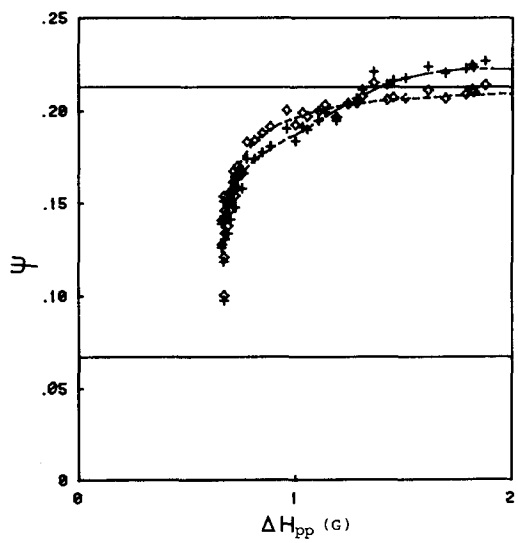

FIG. 5. The line shape parameter ψ of the $M_I = 0$ manifold of DTBN as a function of the overall manifold linewidth. The experimental points are given by + and these points corrected by Appendix (B) to account for interference from ^{14}C satellites are given by ◇. The lines are generated by the equations of Appendix B with and without inclusion of ^{13}C satellites. The horizontal lines correspond to a Gaussian line shape, $\psi^G = 0.067$ and a Lorentzian line shape $\psi^L = 0.213$, respectively. Mesitylene, $T = 30.00$°C.

fined[18] and for Gaussian–Lorentzian mixtures, ψ was found to be a monotonic function of the ratio $\Delta H_{pp}^G/\Delta H_{pp}^L$.

The line shape parameter ψ measured on the same spectra that produced the data in Fig. 3 are plotted as a function of the linewidth in Fig. 5. The two sets of symbols show the result of a correction to take account of the presence of small satellites due to ^{13}C in natural abundance. This correction is discussed in Appendix B.

The two horizontal lines in Fig. 5 show the limits expected for pure Gaussian and Lorentzian, respectively, so we see that the composite line varies from being quite Gaussian to being entirely Lorentzian. Note the very rapid increase in Lorentzian character as a function of the total linewidth. This rapid rise is due to two simultaneous mechanisms in the intermediate exchange region—the Lorentzian linewidth increases and the hyperfine pattern collapses. Both factors increase ψ while they tend to offset one another in their contribution to the overall linewidth.

The lines in Fig. 5 were produced from the theory of Currin by extracting ψ from simulated spectra. It is seen that the agreement of the experimental and theoretical results is good indeed. Similar results are observed for DTBN in *cis*-decalin and *trans*-decalin and equally good agreement with theory is obtained.

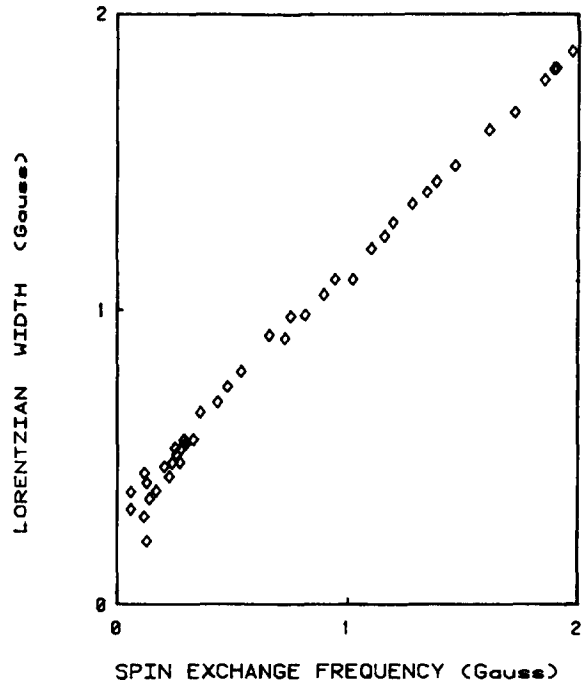

FIG. 6. The Lorentzian component of the $M_I = 0$ manifold of DTBN vs the spin exchange frequency calculated from Eq. (10) of Ref. 18. Mesitylene, $T = 30.00°C$.

DISCUSSION

Utilizing the previous methods[18] ΔH_{pp}^G and ΔH_{pp}^L, the Gaussian and Lorentzian linewidths may be obtained separately once ψ is measured. This deconvolution shown in Figs. 3 and 4 behaves as one would expect—ΔH_{pp}^G tends to decrease as the intensity, and therefore ω_{HE}, increases while ΔH_{pp}^L increases linearly. Obviously ΔH_{pp}^L is an average quantity at slow to intermediate spin exchange frequencies because, as we have already noted, the Lorentzian linewidths vary from line to line.

Is this type of deconvolution meaningful for a line in the intermediate spin exchange region undergoing a complicated shape change? In other words, are the spectral lines, in the spin exchange case, well described by the type of Gaussian–Lorentzian convolutions that accurately describe the lines in the absence of exchange?[18] In the case of DTBN, we have shown this to be so by comparing spectral simulations in the intermediate exchange range with Gaussian–Lorentzian convolutions of the same ψ properly scaled to give the same ΔH_{pp} and spectral intensity. In each case, the exchange influenced spectrum was virtually identical to the Gaussian-Lorentzian convolution.

The worst case that we found was for $\psi = 0.165$ which is in the heart of the intermediate exchange regime (see Fig. 5) where for $\omega_{HE}/a_e(0) = 1.8$ and $T_2^{-1}/a_e(0) = 2.39$ the results differed at most by 1.2% in the wings from the spectrum generated for $\omega_{HE}/a_e(0) = 0$ and $T_2^{-1}/a_e(0) = 5.04$. A figure is not included because it is practically impossible to discern the difference in the two spectra. The latter spectrum is accurately a Gaussian–Lorentzian convolution thus, for practical purposes at least for DTBN, the former is also.

Since this is so, we define an effective hyperfine coupling, as before,[18] which for DTBN would be,

$$a_e(\omega_{HE}) = (1.06n)^{-1/2}\,\Delta H_{pp}^G \,. \tag{3}$$

Thus, the decrease in ΔH_{pp}^G can be interpreted as being due to the lines continuing to move toward one another with an average spacing $a_e(\omega_{HE})$. For such an interpretation to make sense, one would expect ΔH_{pp}^L to vary linearly with ω_{HE}, at least away from the origin. Figures 6 and 7 show the experimental variation of ΔH_{pp}^L vs ω_{HE} for DTBN in two of the solvents. At large ω_{HE}, in the fast exchange limit, the slope of the lines in Figs. 6 and 7 is near the expected $4/3\sqrt{3}$ for a nitroxide while at low ω_{HE} a larger slope is expected and is observed. Note that the line shape of a Lorentzian–Gaussian convolution is completely specified by two parameters so, to the extent that the line shapes in the intermediate exchange regime may be represented by such a convolution, only the two parameters ψ and ΔH_{pp} are required to compare experiment and theory.

From the Gaussian component, the effective hyperfine coupling constant may be derived from Eq. (3). The results for DTBN in all three hydrocarbons studied are plotted in Fig. 8 vs the spin exchange frequency. The theoretical prediction is given as the solid line in Fig. 8 This is an alternative way to compare the line shapes with theory, and the agreement of experiment with theor is quite good throughout the intermediate exchange region. The points in Fig. 8, even though they are within experimental error of the theoretical line, seem to be falling off slightly more rapidly than theory at high spin exchange frequencies but unfortunately it is just this region that is most affected by corrections due to ^{13}C lines rendering the results less certain.

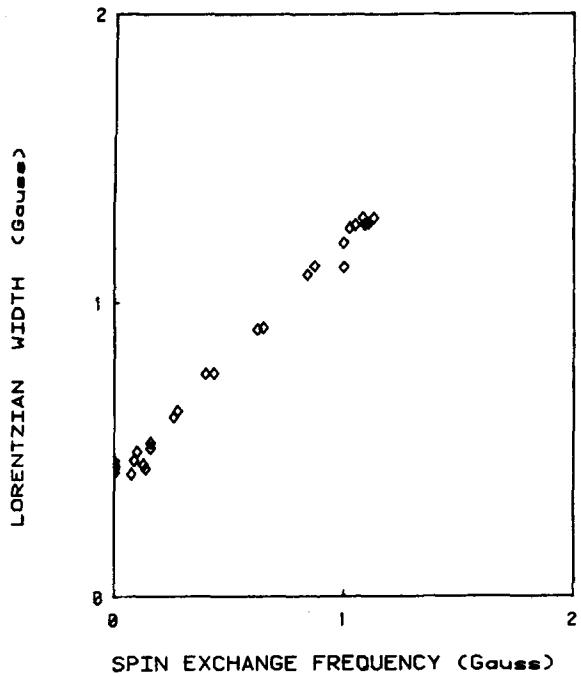

FIG. 7. The Lorentzian component of the $M_I = 0$ manifold of DTBN vs the spin exchange frequency calculated from Eq. (10), of Ref. 18. *Trans*-decalin, $T = 30.00$°C.

Given the interpretation that we have suggested, it is of some interest to consider the rate of collapse as demonstrated by Fig. 8. In order to put the collapse rate into context, we again turn to Currin's theory and plot in Fig. 8 (dotted line) the theoretical collapse of a single multiplet (no nitrogen structure) of 19 lines. Actually, to put the two curves in Fig. 8 on the same footing, the single manifold collapse was calculated using

$$\omega_{HE}(\text{SINGLE}) = \omega_{HE}(\text{NITROXIDE})/3 ,$$

since only one-third of the spin exchanges for nitroxides occur within a given manifold. Clearly, there are qualitative as well as quantitative differences in the collapse rates of a single vs three manifolds. Empirically, the curves are very well represented by

$$\alpha_e(\omega_{HE})_{\text{SINGLE}} = \alpha_e(0)\exp[-\omega_{HE}\ln 2/\alpha_e(0)] ,$$

$$\alpha_e(\omega_{HE})_{\text{NITROXIDE}} = \alpha_e(0)[1+\omega_{HE}/7.9\alpha_e(0)]^{-1} .$$

Intuitively, we expected a rapid collapse of the hyperfine structure in the region of $\omega_{HE} \sim \alpha_e(0)$ and for the single manifold, we see that this is the case. However, the simple intuitive picture does not hold when several manifolds are present—the intermanifold exchanges do more than simply dilute the number of intramanifold exchanges—they change the qualitative behavior of the line shape.

The values of K_e of Eq. (2) were determined by fixing the (arbitrary) intensity to correspond to 6×10^{-3} M at its maximum in each case and then finding the slope of ω_{HE} vs the concentration of DTBN given in moles per liter (see Ref. 21). Linear least squares fits yielded the results for K_e which are given in Table II.

In a simple hydrodynamic model that assumes that

TABLE II. Spin exchange rate constants for DTBN and comparison with simple hydrodynamic theory. $T = 30$°C.

Solvent	$K_e\times10^{-9}$ (ℓ/mol s)	$K_e\eta/T\times10^{-5}$ (P/mol s K)
mesitylene	5.3[a]	1.1
cis-decalin	2.2[a]	1.9
trans-decalin	3.2[a]	1.8
	Hydrodynamic model (stick)	1.11
	Hydrodynamic model (slip)	1.67

[a]Error estimated to be ±10%.

DTBN diffuses as spheres according to the Stokes–Einstein model[12]

$$K_e = \frac{8RT}{6000\eta} , \tag{4}$$

where η is the solvent viscosity, R is the gas constant, giving K_e in units of ℓ/mol s. Equation (4) assumes conditions of strong exchange (diffusion controlled) that the interaction distance is equal to the diameter of the radical, and that so-called "stick" boundary conditions are employed.[27] If "slip" boundary conditions are assumed, then K_e is increased by a factor of 3/2.[27] The condition of strong exchange cannot be demonstrated by a constant temperature experiment but is very likely in these solvents.[12,25] The values of K_e for slip and stick boundary conditions calculated from Eq. (4) are given in Table II together with the experimental results. The viscosity

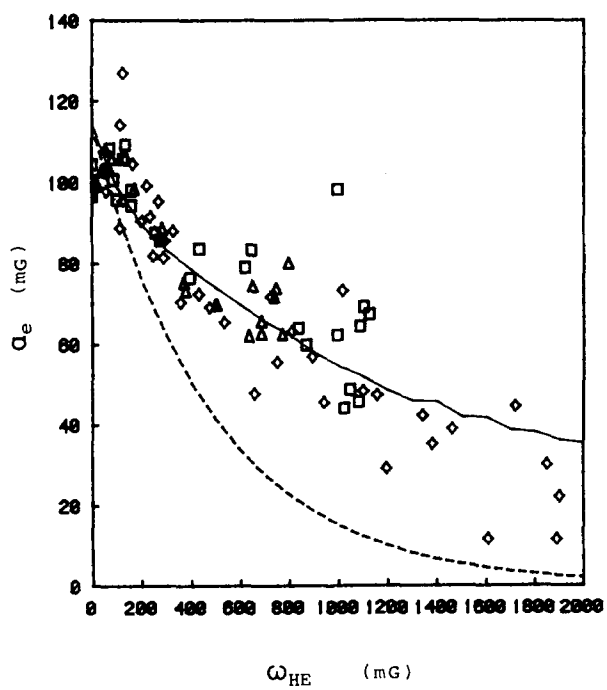

FIG. 8. The effective hyperfine coupling constant vs the spin exchange frequency for DTBN in mesitylene (Δ); *trans*-decalin (◇); and *cis*-decalin (□). The theory of Currin (Ref. 5) produced the solid line. The scatter of the points indicates the uncertainty which is most severe in the 1.3–2.0 G range due to corrections for ^{13}C satellite lines. The dotted line shows Currin's theory for a single manifold of lines but with ω_{HE}(single) = ω_{HE}(nitroxide)/3.

of *cis*-decalin and *trans*-decalin were taken from the literature[26] and the viscosity of mesitylene was measured by Hadley to be 0.615 ± 0.008 cP at $T = 30 \pm 0.1$ °C in this laboratory using a capillary method calibrated with distilled water.

The data in Table II show that the results of spin exchange of DTBN in mesitylene are very well explained by the simple hydrodynamic theory with stick boundary condition while for the two decalins, K_e is similar and nearer to the slip boundary conditions. It has to be borne in mind that these experiments were not carried out with testing of hydrodynamic theory in mind so the data in Table I do not warrant extensive discussion, but the data suggest that such a careful study would be worthwhile. One would work with higher concentrations of the radical in order to measure K_e in the fast exchange limit to increase the precision of the measurements.

Finally, we observe that the measurement of ω_{HE} in the intermediate exchange region could be of practical importance in case neither the fast exchange nor the slow exchange limits were accessible—e.g., if one had limited solubility of the radical or if one wanted to avoid excessively high concentrations in, say, a biological system.

ACKNOWLEDGMENTS

This work was funded in part by Institutional Grant #425712000 from the C.S.U.N. Foundation. We wish to thank Mr. Brian Hadley for the viscosity measurement of mesitylene.

APPENDIX A

The real part of the first derivative of Eq. (1) gives the absorption derivative observed in our experiments. Recalling that H_j denotes the resonance field of the jth line in the hyperfine multiplet $\rho_j = d_j / \sum d_j$, where d_j is the degeneracy of the jth line, and $2T_2^{-1}$ is the width of the individual Lorentzian absorption lines, the spectrum is given by

$$\mathrm{Re}\frac{d}{dH}G(H) = \frac{D_1 N_2 - N_1 D_2}{D_1^2}, \tag{A1}$$

where,

$$D_1 = (\sigma_5)^2 + \omega_{HE}^2(\sigma_4)^2, \tag{A2a}$$

$$D_2 = 2\sigma_5\sigma_6 + 2\omega_{HE}^2\sigma_4\sigma_7, \tag{A2b}$$

$$N_1 = Q\sigma_3\sigma_5 - \omega_{HE}(\sigma_4)^2, \tag{A2c}$$

$$N_2 = Q(\sigma_3\sigma_6 - 2\sigma_1\sigma_5) - 2\omega_{HE}\sigma_4\sigma_7, \tag{A2d}$$

where $Q \equiv \omega_{HE} + T_2^{-1}$. With the further definitions $C_j(H) \equiv H - H_j$ and

$$L_j \equiv \{[C_j(H)]^2 + Q^2\}^{-1}$$

the sums in Eqs. (A2a)–(A2d) are given by

$$\sigma_1 = \sum \rho_j C_j L_j^2, \quad \sigma_2 = \sum \rho_j C_j^2 L_j^2, \quad \sigma_3 = \sum \rho_j L_j,$$

$$\sigma_4 = \sum \rho_j C_j L_j, \quad \sigma_5 = 1 - \omega_{HE} Q \sigma_3,$$

$$\sigma_6 = 2\omega_{HE} Q \sigma_1, \quad \sigma_7 = \sigma_3 - 2\sigma_2,$$

where the sums are over all of the lines in the hyperfine multiplet. Undoubtedly, Eq. (A1) may be simplified algebraically somewhat, but in its present form, it is easily programmed on a minicomputer. The program written for an Apple computer will be supplied upon request by the authors.

To the level of approximation that includes consideration of a single set of ^{13}C satellites (see Appendix B) the above sums would extend over 19 lines in each of three manifolds and 19 lines in each of six satellites for a total of 171 lines. Fortunately, by designing the range of ω_{HE} and T_2^{-1} properly, one can reduce the number of lines required in the simulation substantially. First we take advantage of the fact that the three manifolds are separated by the nitrogen hyperfine coupling constant which, being of order 15 G is much larger than the total manifold linewidth as long as ω_{HE} and T_2^{-1} are not too large. Thus, under appropriate circumstances, we may neglect manifold overlap and treat one manifold of lines at a time. This is accomplished by setting the nitrogen hyperfine coupling constant, a_N to infinity which, in effect, means that the above sums are over the lines in one manifold remembering that the remaining ρ_j are normalized to 1/3.

Comparing full simulation and those neglecting manifold overlap shows that the linewidth is affected less than 1% and ψ less than 2% up to linewidths of 2.28 G $\sim 0.15 a_N$. The matter of overlap affects a_e more—in Fig. 8 at a linewidth of 1.5 G, one deduces $a_e = 0.041$ G neglecting overlap and $a_e = 0.044$ G including it while at a linewidth of 1.8 G, the respective values are $a_e = 0.034$ and 0.047 G. Under normal circumstances we would have made corrections for a_e due to overlapping manifolds above linewidth of 1.5 G, but in this region both experimental uncertainty and the corrections due to ^{13}C satellites made these corrections moot. Above linewidths of 1.8 G, the errors in a_e due to neglect of manifold overlap become very serious so we have limited our experimental work to the range of T_2^{-1} and ω_{HE} which yielded linewidths less than this value.

Thus, most of the simulations in this work extended over 19 main lines in one manifold plus or minus 38 lines in the ^{13}C satellites.

APPENDIX B: CORRECTIONS FOR ^{13}C SATELLITES

The intensity of the ^{13}C satellites is small compared with the main line intensity, so for most purposes the satellite's presence would be inconsequential. As luck would have it, however, in part of the range of linewidths that interest us, the small perturbation of the intensity in the wings of the line is enough to affect the extraction of $a_e(\omega_{HE})$ from ψ even though ψ itself is not greatly affected (see Fig. 5). Fortunately, correction for these satellites is straightforward and is rendered easier by the fact that, in hydrocarbons, the hyperfine coupling constants to the α and β carbons in DTBN, respectively, $\alpha(^{13}C_\alpha)$ and $\alpha(^{13}C_\beta)$, happen to be equal.[28] Using our measured ^{14}N hyperfine coupling constants and an empirical equation given by Rassat and coworkers,[28] we calculate ^{13}C hyperfine coupling constants given in Table I. Actually, computer simulations at

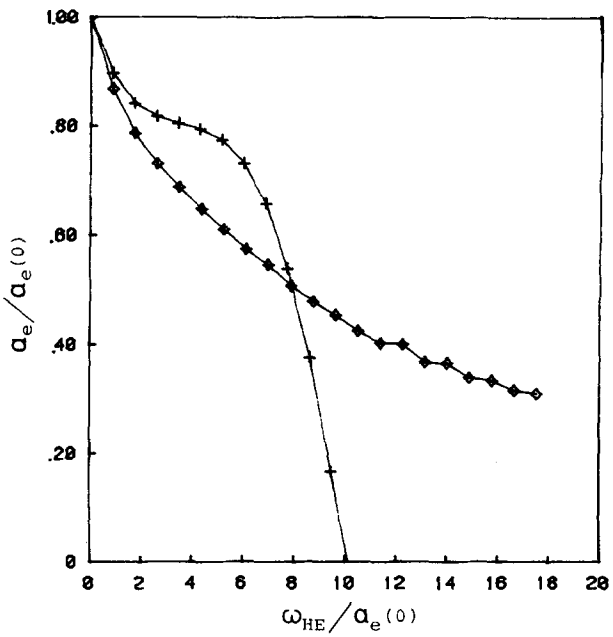

FIG. 9. The effect of corrections for ^{13}C satellite lines on $a_e(\omega_{HE})$. The points were derived from simulated spectra without (◇) and with (+) the satellites included.

$\omega_{HE}=0$ fit better with $\alpha(^{13}C)=4.12$ G, so this value and a satellite-to-main-line-intensity ratio of 0.0448, calculated assuming eight equivalent ^{13}C sites, were used in all of the calculations. A total of 57 lines are involved in the sums of Appendix A—19 in the main lines were Lorentzian of equal width spaced appropriately at $\omega_{HE}=0$ using the $\alpha_e(0)$ coupling and T_2^{-1} given in Table I. Each of the 38 lines in the satellites has an intensity equal to 0.0448 of the corresponding line in the main manifold and $\sum \rho_j = 1/3$ summed over all 57 lines.

Spectra were generated at various T_2^{-1}, and ω_{HE} and ψ was extracted from the simulation. Call this parameter with the satellites included ψ^* and without the satellites ψ. In the experiment, one measures ψ^* and wishes to ascertain ψ so we write $\psi=\psi^*+\psi_c$ and find that the correction term may be approximated by

$$\psi_c=\sum_{j=0}^{4} a_j(\Delta H_{pp})^j\ , \tag{B1}$$

where $a_0=0.26404$, $a_1=-0.85541$, $a_2=0.92738$, $a_3=-0.40808$, and $a_4=0.06333$, with coefficient of correlation $r=0.9983$ over the range $\Delta H_{pp}=0.66$ to 1.83 G. The correction was generated using $T_2^{-1}=0.265$ G and $a_e(0)=0.111$ G, but the correction is not very sensitive to these values.

The effect of the ^{13}C satellites on ψ is shown in Fig. 5, which is not severe but the effect on $a_e(\omega_{HE})$ is shown in Fig. 9 and is seen to change its quantitative and qualitative behavior. We have chosen to apply the correction of Eq. (B1) to the experimental data and compare those with the theory, removing the satellite interference, in Fig. 8.

As a practical matter, the ^{13}C satellites hardly ever need to be a concern. If $a_e(0)$ is known, or is determined experimentally from ψ^* at $\Delta H_{pp}<0.72$ G, then Eq. (B2) of Ref. 18(b) gives ΔH_{pp}^L to better than 2.4% at all linewidths.

It should be mentioned that the correction in Eq. (B1) involves more than just the superposition of satellites situated at $\pm a(^{13}C)/2$ and of the same shape and width as the main line—the satellites broaden faster than the main line and begin to move inward. A straightforward superposition would be obtained if the lines were broadened by a different exchanging paramagnetic species or by any other mechanism which would increase T_2^{-1} without collapsing the hyperfine structure. For reference, we include the correction for this latter case as

$$\psi_c=\sum_{j=0}^{4} b_j(\Delta H_{pp})^j\ , \tag{B2}$$

with $b_0=-0.11153$, $b_1=0.63776$, $b_2=-1.1554$, $b_3=0.79572$, and $b_4=-0.18129$ with $r=0.9994$. Equation (B2) was generated using $\omega_{HE}=0$ and $a_e(0)=0.111$ G varying T_2^{-1} such that ΔH_{pp} varied from 0.65 to 1.77 G.

[1]See, for example, C. S. Johnson, Jr., in *Advances in Magnetic Resonance*, edited by J. S. Waugh (Academic, New York, 1965), Vol. 1.
[2]P. W. Anderson, J. Phys. Soc. Jpn. **9**, 316 (1954).
[3]G. E. Pake and T. R. Tuttle, Jr., Phys. Rev. Lett. **3**, 423 (1959).
[4]D. Kivelson, J. Chem. Phys. **33**, 1094 (1960).
[5]J. D. Currin, Phys. Rev. **126**, 1995 (1962).
[6]C. S. Johnson, Jr., Mol. Phys. **12**, 25 (1967).
[7]J. H. Freed, J. Chem. Phys. **45**, 3452 (1966).
[8]J. H. Freed, J. Phys. Chem. **71**, 38 (1967).
[9]A. E. Stillman and R. N. Schwartz, J. Magn. Reson. **22**, 269 (1976).
[10]W. Plachy and D. Kivelson, J. Chem. Phys. **47**, 3312 (1967).
[11]M. P. Eastman, R. G. Kooser, M. R. Das, and J. H. Freed, J. Chem. Phys. **51**, 2690 (1969).
[12]M. P. Eastman, G. V. Bruno, and J. H. Freed, J. Chem. Phys. **52**, 2511 (1970).
[13]A. L. Kovarskii, A. M. Wasserman, and A. L. Buchachenko, J. Magn. Reson. **7**, 225 (1972).
[14]B. L. Bales, J. A. Swenson, and R. N. Schwartz, Mol. Cryst. Liq. Cryst. **28**, 143 (1974).
[15]T. A. Miller, R. N. Adams, and P. M. Richards, J. Chem. Phys. **44**, 4022 (1966).
[16]Two nuclei are "completely" equivalent if their hyperfine splittings are the same at any instant. See, J. H. Freed and G. K. Fraenkle, J. Chem. Phys. **39**, 326 (1963).
[17]*Spin Labeling Theory and Applications*, edited by L. J. Berliner (Academic, New York, 1975).
[18](a) B. L. Bales, J. Magn. Resonance **38**, 193 (1980); (b) **48**, 418 (1982).
[19]We are grateful to the referee who pointed out that Freed's theory can be cast into the Form of Eq. (1) by solving the coupled equations.
[20]R. B. Clarkson, Varian VIA **13**, 4 (1979).
[21]B. L. Bales and D. Willett, J. Magn. Reson. **51**, 138 (1983).
[22]G. Poggi and C. S. Johnson, Jr., J. Magn. Reson. **3**, 436 (1970).
[23]A. K. Hoffman, J. Am. Chem. Soc. **86**, 641 (1964).
[24]R. J. Faber, F. W. Markley, and J. A. Weil, J. Chem. Phys. **46**, 1652 (1967).
[25]J. C. Lang and J. H. Freed, J. Chem. Phys. **56**, 4103 (1970).
[26]D. L. Hogenboom, W. Webb, and J. A. Dixon, J. Chem. Phys. **46**, 2586 (1967).
[27]See, for example, L. L. Jones and R. N. Schwartz, Mol. Phys. **43**, 527 (1981), and references therein.
[28]R. Briere, G. Chapelet-Letourneux, H. Lemaire, and A. Rassat, Mol. Phys. **20**, 211 (1971).